

## On the Origin of the Cation Templated Self-Assembly of Uranyl-Peroxide Nanoclusters

Pere Miró, Simon Pierrefixe, Mickaël Gicquel, Adrià Gil, and Carles Bo\*

Institute of Chemical Research of Catalonia, ICIQ, Avda. Països Catalans 16, 43007 Tarragona,  
Spain and Departament de Química Física i Inorgànica, Universitat Rovira i Virgili,  
Campus Sescelades, Tarragona, Spain

Received June 17, 2010; E-mail: cbo@iciq.es

**Abstract:** Uranyl-peroxide nanoclusters display different topologies based on square, pentagonal and hexagonal building blocks. Computed complexation energies of different cations ( $\text{Li}^+$ ,  $\text{Na}^+$ ,  $\text{K}^+$ ,  $\text{Rb}^+$ , and  $\text{Cs}^+$ ) with  $[\text{UO}_2(\text{O}_2)(\text{H}_2\text{O})]_n$  ( $n = 4, 5$ , and  $6$ ) macrocycles suggest a strong cation templating effect. The inherent bent structure of a  $\text{U}-\text{O}_2-\text{U}$  model dimer is demonstrated and justified through the analysis of its electronic structure, as well as of the inherent curvature of the four-, five-, and six-uranyl macrocycles. The curvature is enhanced by cation coordination, which is suggested to be the driving force for the self-assembly of the nanocapsules.

### Introduction

The self-assembly of uranium polyhedra into a wide variety of nanoclusters containing up to 60 uranium atoms has been described very recently by Burns and co-workers.<sup>1–7</sup> This new family of uranyl-peroxide nanoclusters, obtained under favorable conditions in an alkaline peroxide environment, is unique in actinide chemistry. In the last couple of years, numerous uranyl-peroxide nanoclusters, designated  $\text{U}_n$  (where  $n$  is the number of uranium polyhedra), have been reported:  $\text{U}_{20}$ ,  $\text{U}_{24}$ ,  $\text{U}_{28}$ ,  $\text{U}_{32}$ ,  $\text{U}_{36}$ ,  $\text{U}_{40}$ ,  $\text{U}_{44}$ ,  $\text{U}_{50}$ , and  $\text{U}_{60}$ . In all cases, the polyhedron is a hexagonal bipyramid, the apexes of which correspond to the oxygen atoms of the uranyl cation  $[\text{UO}_2]^{2+}$ . The hexagonal bipyramids then bind each other by sharing equatorial edges with adjacent polyhedra and form units containing 4, 5, or 6 polyhedra in square (**S**), pentagonal (**P**), or hexagonal (**H**) arrangements, respectively (Figure 1). These units, which self-assemble a posteriori, constitute the basic building blocks from which the nanoclusters are then built up. Due to the possibility of forming peroxide ( $\mu\text{-O}_2$ ) or hydroxide ( $\mu\text{-OH}$ )<sub>2</sub> bridges between the uranium atoms, several types of faces are observed: fully peroxide and mixed peroxide-hydroxide faces.<sup>1</sup>

Some of the recently described structures present a topology that is similar to that of carbon-based fullerenes.<sup>8</sup> The most remarkable example,  $[\text{UO}_2(\text{O}_2)(\text{OH})]_{60}^{60-}$ , in analogy with  $\text{C}_{60}$ , is comprised of 12 pentagonal peroxide-bridged building blocks  $[\text{UO}_2(\text{O}_2)]_5$  and of 30  $(\text{OH})_2$  linkers forming hexagonal faces that connect the pentagons together.<sup>4</sup> Also, in a very recently reported new  $\text{U}_{60}$  cluster,<sup>7</sup> the  $(\text{OH})_2$  linkers are replaced by oxalate ligands. However, despite some similarities, uranyl-peroxide nanoclusters tend to favor high symmetry over the minimal pentagonal adjacency rule found in fullerene chemistry. Furthermore, no square arrangements of carbon atoms are found in fullerene chemistry. Similarly, one can also relate the uranyl-peroxide nanoclusters to giant polyoxometalates (POMs).<sup>9,10</sup> For example, the spherical nanocapsule  $\text{Mo}_{132}$  is an inorganic superfullerene built up by 12 pentagonal  $\text{Mo}(\text{Mo}_5)$  units and 30  $\text{Mo}_2$  linkers.<sup>11</sup> This observation highlights the crucial role of stable pentagonal building blocks in the formation of spherical nanoclusters.

This new class of uranium compounds provides exciting prospects in nuclear waste treatment and in nanotechnology. Unfortunately, subtle changes in growth conditions result in dramatic changes in the type of nanoclusters obtained. Therefore, we need to understand the mechanism by which the clusters form, to tune the size and topology of the nanoclusters during synthesis. In this respect, the influence of the alkali cations used during the synthesis seems to be critical. Indeed, the X-ray diffraction of uranium nanocapsules revealed that the alkali cations are located only under the center of fully peroxide faces

- (1) Burns, P. C.; Kubatko, K.-A.; Sigmon, G.; Fryer, B. J.; Gagnon, J. E.; Antonio, M. R.; Soderholm, L. *Angew. Chem., Int. Ed.* **2005**, *44* (14), 2135–2139.
- (2) Forbes, T. Z.; McAlpin, J. G.; Murphy, R.; Burns, P. C. *Angew. Chem., Int. Ed.* **2008**, *47* (15), 2824–2827.
- (3) Sigmon, G. E.; Ling, J.; Unruh, D. K.; Moore-Shay, L.; Ward, M.; Weaver, B.; Burns, P. C. *J. Am. Chem. Soc.* **2009**, *131* (46), 16648–16649.
- (4) Sigmon, G. E.; Unruh, D. K.; Ling, J.; Weaver, B.; Ward, M.; Pressprich, L.; Simonetti, A.; Burns, P. C. *Angew. Chem., Int. Ed.* **2009**, *48* (15), 2737–2740.
- (5) Sigmon, G. E.; Weaver, B.; Kubatko, K. A.; Burns, P. C. *Inorg. Chem.* **2009**, *48* (23), 10907–10909.
- (6) Ling, J.; Qiu, J.; Sigmon, G. E.; Ward, M.; Szymanowski, J. E. S.; Burns, P. C. *J. Am. Chem. Soc.* **2010**, *132*, 13395–13402.
- (7) Ling, J.; Wallace, C. M.; Szymanowski, J. E. S.; Burns, P. C. *Angew. Chem., Int. Ed.* **2010**, *49*, 7271–7273.
- (8) Fowler, P. W.; Manolopoulos, D. E. *An Atlas of Fullerenes*; Oxford University Press: Oxford, 1995.
- (9) Pope, M. T.; Müller, A. *Polyoxometalate Chemistry: From Topology Via Self-Assembly to Applications*; Kluwer Academic Publishers: Dordrecht, 2001.
- (10) Long, D. L.; Tsunashima, R.; Cronin, L. *Angew. Chem., Int. Ed.* **2010**, *49* (10), 1736–1758.
- (11) Müller, A.; Sarkar, S.; Shah, S. Q. N.; Bogge, H.; Schmidtmann, M.; Sarkar, S.; Kogerler, P.; Hauptfleisch, B.; Trautwein, A. X.; Schunemann, V. *Angew. Chem., Int. Ed.* **1999**, *38* (21), 3238–3241.

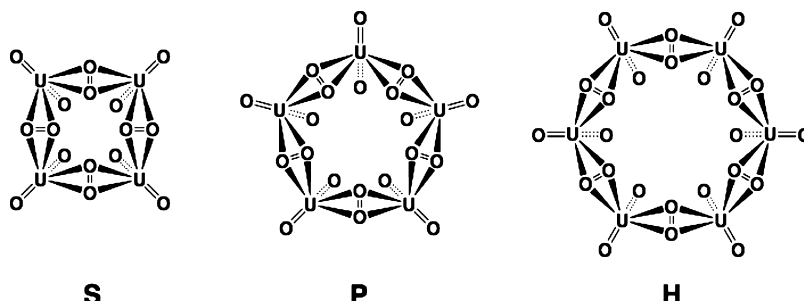


**Figure 1.** Schematic representations of peroxide-bridged  $[(\text{U}^{\text{VI}}\text{O}_2)_4(\text{O}_2)_4]$  (**S**),  $[(\text{U}^{\text{VI}}\text{O}_2)_5(\text{O}_2)_5]$  (**P**), and  $[(\text{U}^{\text{VI}}\text{O}_2)_6(\text{O}_2)_6]$  (**H**). View from the concave side of the ring.

**Table 1.** Fully Peroxide Face, **S** (Square), **P** (Pentagonal), and **H** (Hexagonal) Observed Experimentally in Some Uranyl-Peroxide Nanoclusters and the Corresponding Alkali Cations Used during Synthesis<sup>a</sup>

$\text{U}_n$	$\text{U}_{20}$	$\text{U}_{24}$	$\text{U}_{28}$	$\text{U}_{40}$	$\text{U}_{44}$	$\text{U}_{60}$
faces	<b>P</b>	<b>S</b>	<b>P, H</b>	<b>S</b>	<b>P</b>	<b>P</b>
cations	$\text{Na}^+$	$\text{Li}^+$	$\text{K}^+$	$\text{Na}^+$	$\text{Na}^+/\text{K}^+$	$\text{K}^+$

<sup>a</sup>  $\text{U}_{32}$ ,  $\text{U}_{36}$ , and  $\text{U}_{50}$  were left out because no cation has been observed experimentally.

inside the nanoclusters, coordinated to the uranyl oxygens, but in a discriminate manner: square faces are coordinated to  $\text{Li}^+$  or  $\text{Na}^+$ , whereas pentagonal faces coordinate to  $\text{Na}^+$  or  $\text{K}^+$  (see Table 1). Only in one case,  $\text{U}_{28}$ ,<sup>1</sup> potassium cations are observed under the hexagonal faces. In a related system, a square  $[\text{UO}_2(\text{O}_2)]_4$  face was isolated by Kortz's group in a polyoxo tungsto phosphate,<sup>12</sup> which precisely holds a  $\text{Li}^+$  in the center of the square. The aforementioned experimental results drove us to ponder on the higher stability of the isolated fully peroxide-bridged building blocks, and on the template effect of the alkali cations, which is closely related to macrocycle-based systems in inorganic supramolecular chemistry and to the selective cation complexation in POMs.<sup>13</sup> In a broad sense, this is also related to the anion templated self-assembly of helicates.<sup>14,15</sup> Our hypothesis is strengthened by the fully peroxide cluster fragments containing 2, 5, and 6 uranyl polyhedra recently characterized by Sigmon et al.<sup>3</sup>

Here, we present a theoretical study aimed at providing evidence of the inherent bent structure and stability of the isolated building blocks. Also, we will prove that the fully peroxide **S** and **P** face topologies prefer to coordinate to certain alkali cations rather than to others, and we will demonstrate the geometrical flexibility of **H**.

## Computational Details

All DFT calculations were performed using the Amsterdam Density Functional program (ADF2008) developed by Baerends, Ziegler, and co-workers.<sup>16</sup> We used the local VWN exchange-

correlation potential<sup>17</sup> with nonlocal Becke's exchange correction<sup>18</sup> and Perdew's correlation correction<sup>19,20</sup> (BP86). Relativistic corrections were introduced by scalar-relativistic zero-order regular approximation<sup>21</sup> (ZORA). A triple- $\zeta$  plus two polarization functions basis set was used on all atoms. For non-hydrogen atoms, a relativistic frozen-core potential was used. Solvent effects were introduced by using the continuous solvent model COSMO<sup>22</sup> with Allinger radii<sup>23</sup> for Na and K. Indeed, the Bragg radius<sup>24</sup> reproduces best the experimental solvation energy in the case of Li, Rb, and Cs, while Allinger gives better results for the rest of cations (see Table S1 of the SI). Geometries were fully optimized without any symmetry constraints, and characterized by harmonic vibrational analysis. Some structures presented very low imaginary frequencies (below 15  $\text{cm}^{-1}$ ) corresponding to orientational motion of ligand water molecules. Only in the case of the model dimer,  $D_{2h}$  or  $C_{2v}$  symmetry was imposed. ELF (Electron Localization Function)<sup>25,26</sup> analyses were carried out by using the TopMoD package.<sup>27</sup>

**Origin of the Bent  $\text{U}-(\text{O}_2)-\text{U}$  Dimer.** Sigmon<sup>3</sup> et al. reported the X-ray structure for the  $\text{K}_6[(\text{UO}_2)_2(\mu-\eta^2:\eta^2-\text{O}_2)(\text{C}_2\text{O}_4)_4]$  dimer, the smallest system containing the  $\text{U}-(\mu-\eta^2:\eta^2-\text{O}_2)-\text{U}$  peroxide bridge unit, which is bent along the O–O peroxide bond and the oxo-uranyl atoms of which are in axial positions with respect to the uranyl coordination main plane. This system has been studied very recently by Vlaisavljevich et al.,<sup>28</sup> who found that the bent angle depends on the size and electronegativity of the counterions. We considered as a model system the cationic  $[(\text{UO}_2)_2(\mu-\eta^2:\eta^2-\text{O}_2)(\text{H}_2\text{O})_6]^{2+}$  dimer depicted in Figure 2, which reproduces fairly well the basic structural features of the X-ray reported data.<sup>3</sup> For instance, some X-ray vs computed (between parentheses) geometrical parameters:  $\text{U}-\text{O}_{\text{oxo}} = 1.793$  (1.801), 1.789 (1.800);  $\text{O}-\text{O}_{\text{peroxy}} = 1.473$  (1.444);  $\text{U}-\text{O}_{\text{peroxy}} = 2.314$  (2.342);  $\text{U}-\text{U} = 4.309$  (4.238); dihedral  $\text{U}-\text{O}_2-\text{U} = 153.0$  (143.9), reveal the inherent bent structure of the  $\text{U}-(\text{O}_2)-\text{U}$  unit. The  $\text{U}-(\text{O}_2)-\text{U}$  unit is highly flexible since an idealized planar  $D_{2h}$  structure lies only 0.5  $\text{kcal}\cdot\text{mol}^{-1}$  above the more stable bent one. Figure 3 shows the frontier molecular orbitals and how they evolve from the  $D_{2h}$  to the  $C_{2v}$  geometry. First, the electronic structure of the uranyl peroxide unit corresponds to that of a classical fully oxidized

- (12) Mal, S. S.; Dickman, M. H.; Kortz, U. *Chem.—Eur. J.* **2008**, *14* (32), 9851–9855.
- (13) Müller, A.; Sousa, F. L.; Merca, A.; Bögge, H.; Miró, P.; Fernández, J. A.; Poblet, J. M.; Bo, C. *Angew. Chem., Int. Ed.* **2009**, *48* (32), 5934–5937.
- (14) Hasenknopf, B.; Lehn, J.-M.; Kneisel, B. O.; Baum, G.; Fenske, D. *Angew. Chem., Int. Ed.* **1996**, *35* (16), 1838–1840.
- (15) Hasenknopf, B.; Lehn, J.-M.; Boumediene, N.; Dupont-Gervais, A.; Van Dorsselaer, A.; Kneisel, B.; Fenske, D. *J. Am. Chem. Soc.* **1997**, *119* (45), 10956–10962.
- (16) Velde, G. T.; Bickelhaupt, F. M.; Baerends, E. J.; Guerra, C. F.; Van Gisbergen, S. J. A.; Snijders, J. G.; Ziegler, T. *J. Comput. Chem.* **2001**, *22* (9), 931–967.
- (17) Vosko, S. H.; Wilk, L.; Nusair, M. *Can. J. Phys.* **1980**, *58* (8), 1200–1211.
- (18) Becke, A. D. *Phys. Rev. A* **1988**, *38* (6), 3098–3100.
- (19) Perdew, J. P. *Phys. Rev. B* **1986**, *33* (12), 8822–8824.
- (20) Perdew, J. P. *Phys. Rev. B* **1986**, *34* (10), 7406–7406.
- (21) van Lenthe, E.; Ehlers, A.; Baerends, E. J. *J. Chem. Phys.* **1999**, *110* (18), 8943–8953.
- (22) Klamt, A.; Schuurmann, G. *J. Chem. Soc., Perkin Trans. 2* **1993**, (5), 799–805.
- (23) Allinger, N. L.; Yuh, Y. H.; Lii, J. H. *J. Am. Chem. Soc.* **1989**, *111* (23), 8551–8566.
- (24) Bragg, W. L. *Philos. Mag.* **1920**, (40), 169.
- (25) Becke, A.; Edgecombe, K. E. *J. Chem. Phys.* **1990**, (92), 5379.
- (26) Silvi, B.; Savin, A. *Nature* **1994**, *371*, 683.
- (27) Noury, S.; Krokidis, X.; Fuster, F.; Silvi, B. *J. Comput. Chem.* **1999**, *23*, 597.
- (28) Vlaisavljevich, B.; Gagliardi, L.; Burns, P. C. *J. Am. Chem. Soc.* **2010**, *132*(41), 14503–14508.

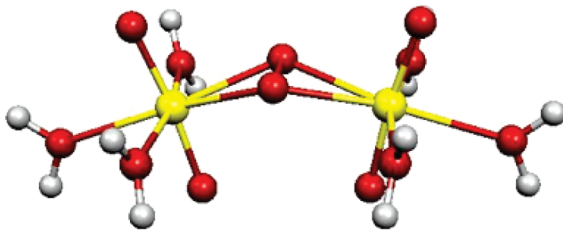


**Figure 2.** Molecular structure of the cationic  $[(\text{UO}_2)_2(\mu-\eta^2:\eta^2-\text{O}_2)(\text{H}_2\text{O})_6]^{2+}$  dimer.

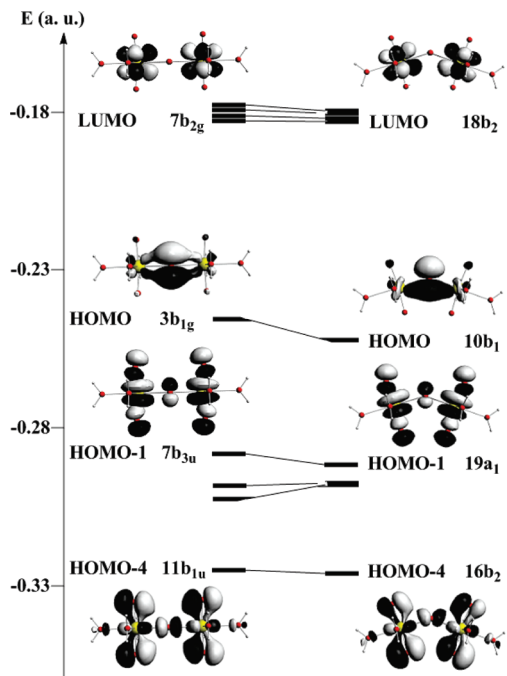


**Figure 3.** Frontier molecular orbitals for  $[(\text{UO}_2)_2(\mu-\eta^2:\eta^2-\text{O}_2)(\text{H}_2\text{O})_6]^{2+}$ ,  $D_{2h}$  (left) vs  $C_{2v}$  (right).

polyoxometalate,<sup>29</sup> i.e., metal valence orbitals (f uranium orbitals) conform the first set of empty energy levels, while the highest occupied orbitals belong to the oxo and peroxy groups. The HOMO is a bonding combination of the peroxy  $\pi^*$  orbital and the uranium atoms, while the HOMO-1 is  $\sigma$ -bonding p oxo ligand with  $f_{z^2}$ -like uranium, and  $\pi$ -antibonding with respect to the peroxy bridge  $\pi$  orbital. The interaction between the uranium atoms and the terminal uranyl oxygen atoms presents a strong covalent character, which reflects the stability of the  $\text{UO}_2^{2+}$  moiety. The next occupied orbitals are mainly lone pairs of the terminal oxo atoms (see Figure 3 and SI) with little contribution of f metal orbitals. In the HOMO, the overlap between the lobes of the  $\pi^*$  peroxy orbital and the  $f_{xyz}$  metal atoms is symmetry allowed, but by bending the  $\text{U}-(\text{O}_2)-\text{U}$  unit, the overlap between the peroxy bridge and the uranium atoms is enhanced, as reflected in Figure 3, and the stability gain is clear. On the contrary, in the HOMO-1, bending reduces the antibonding interaction with the bridge. Globally, the stability gain is reflected in the electronic structure. Analysis of the electronic localization function ELF<sup>25,26</sup> (see Figure 4) revealed that  $\text{U}-\text{O}_2-\text{U}$  bending affects strongly the electronic structure of the peroxy unit. Indeed, ELF attractors of the free  $\text{O}_2^{2-}$  peroxy show two attractors weakly populated (0.2 e) between the two oxygen atoms that indicate ionic O–O bonding. The valence electrons are then mainly localized in the basin of nonbonding valence attractors (6.7 e). This sort of ionic character for the O–O bond is observed in the structures of the

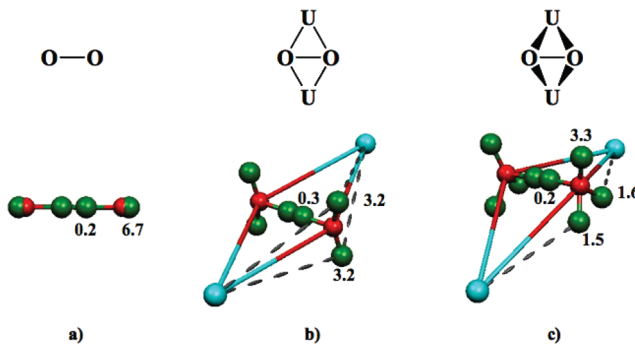


**Figure 4.** ELF valence oxygen attractors (green) and electronic population of  $\text{O}_2^{2-}$  (a),  $[(\text{UO}_2)_2(\mu-\eta^2:\eta^2-\text{O}_2)(\text{H}_2\text{O})_6]^{2+}$   $D_{2h}$  (b) and  $C_{2v}$  (c). Core attractors are respectively blue and red for uranium and oxygen atoms.

dimer as well. The nonbonding valence basin of  $\text{O}_2^{2-}$  is then split into two or three basins for the  $D_{2h}$  and  $C_{2v}$  uranyl complexes, respectively. The attractors between oxygen atoms adopt then  $sp^2$  hybridization in  $D_{2h}$ , and  $sp^3$  hybridization in  $C_{2v}$ , which favors the U–O interaction. Note that the total electronic population of the oxygen atoms keeps nearly constant with respect to that of an isolated peroxy unit, thus indicating that the charge transfer to the uranyl units is small. Consequently, the interaction of the peroxy bridge and the uranyl units is mainly ionic, with some covalent character that is enhanced because of the bending.

**Square and Pentagonal  $[\text{UO}_2(\mu-\eta^2:\eta^2-\text{O}_2)(\text{H}_2\text{O})]_n$  Building Blocks.** We undertook this study by extracting fully peroxy square and pentagonal faces of formula  $[\text{U}^{VI}\text{O}_2(\mu-\eta^2:\eta^2-\text{O}_2)]_n$  where  $n = 4$  and 5 from the X-ray data available. These building blocks present similar features: (i) the uranium atoms are all contained on one plane, (ii) the peroxy bridges ( $\text{O}\alpha, \text{O}\alpha'$ ) connecting the uranium atoms are out of this plane as in the dimer, hence the bent dihedral angle  $\text{U}-(\text{O}_2)-\text{U}$ , (iii) the axes of the uranyl moieties are not perpendicular to the uranium atoms plane but tilted, with one set of the oxygen atoms ( $\text{O}\beta$ ) slightly pointing toward the center of the polygon in order to maximize the interaction with the alkali cation. This leads to shorter  $\text{O}\beta-\text{O}\beta$  distances where the tilting occurs, see Figure 5, thus the  $\text{U}-(\text{O}_2)-\text{U}$  units are bent and twisted.

Then we added one water molecule to each uranium atom of the **S** and **P** building blocks in order to somehow mimic the coordination number of the uranium atoms in the nanocapsules. Thus we studied the macrocycles of formula  $[\text{U}^{VI}\text{O}_2(\mu-\text{O}_2)(\text{H}_2\text{O})]_n$  where  $n = 4$  and 5 for **S** and **P**, respectively, and their corresponding complexes with various alkali cations ( $\text{Li}^+, \text{Na}^+, \text{K}^+, \text{Rb}^+$ , and  $\text{Cs}^+$ ) coordinated to the uranyl  $\text{O}\beta$  oxygen atoms. These structures were optimized without imposing any symmetry constraints.

First, we checked the performance of our DFT approach by comparing X-ray geometrical parameters to their computed counterparts, and we chose **S**( $\text{Li}^+$ ) and **P**( $\text{K}^+$ ) extracted from  $\text{U}_{24}$  and  $\text{U}_{60}$ , respectively. We also determined the geometry of bare **S** and **P** macrocycles to examine the influence of the cation. Although no symmetry constraints were imposed, the resulting optimized structures look like  $C_{4v}$  for **S**( $\text{Li}^+$ ) and  $C_{5v}$  for **P**( $\text{K}^+$ ), with the cation sitting in the center of the ring, and below the plane defined by the  $\text{O}\beta$  oxygen atoms, as in Figure 5. Selected geometrical parameters of interest (experimental and computed) are collected in Table 2. The computed distances are in very good agreement with the experimental data, with discrepancies between 0.01 and 0.11 Å in the interatomic distances. This is true even if no cation is coordinated except in the case of the  $\text{O}\beta-\text{O}\beta$  distances between the oxygen atoms of the uranyl moiety. These distances, crucial to the coordination of the cation to the macrocycle, fluctuate significantly depending on whether a cation is in contact or not. For **S**, there is a deviation of 0.26 Å in the  $\text{O}\beta-\text{O}\beta$  distance when no cation is coordinated, whereas the deviation is of only 0.04 Å if  $\text{Li}^+$  is bound to **S**. Similarly, there is a deviation of 0.39 Å for **P** when no cation is present, whereas the deviation is of only 0.01 Å

(29) Poblet, J. M.; López, X.; Bo, C. *Chem. Soc. Rev.* **2003**, 32 (5), 297–308.

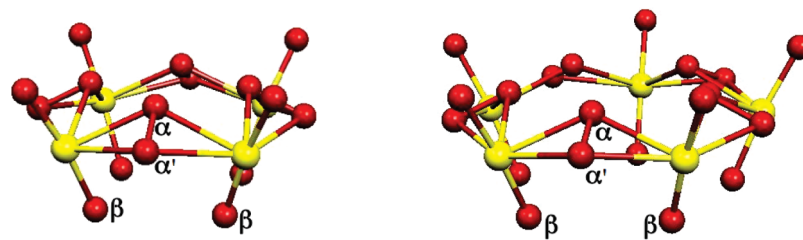


**Figure 5.** Molecular structures of  $[(\text{UO}_2)_4(\text{O}_2)_4]$  (**S**) and  $[(\text{UO}_2)_5(\text{O}_2)_5]$  (**P**) building blocks. Water molecules coordinated to U atoms are omitted for clarity. Uranium yellow, Oxygen red.

**Table 2.** Experimental (X-ray) and Computed (DFT) Geometrical Parameters of Interest (in Å and deg) of **S**, **S**( $\text{Li}^+$ ), **P**, and **P**( $\text{K}^+$ )<sup>a</sup>

faces	<b>S</b>			<b>P</b>		
	cations	$\emptyset$	$\text{Li}^+$	$\emptyset$	DFT	$\text{K}^+$
method	DFT	DFT	X-ray	DFT	DFT	X-ray
U–U	4.19	4.15	4.20	4.33	4.27	4.29
U–O $\alpha$	2.36	2.35	2.37	2.35	2.35	2.39
U–O $\beta$	1.83	1.82	1.79	1.82	1.82	1.84
O $\alpha$ –O $\alpha'$	1.45	1.45	1.54	1.46	1.46	1.47
O $\beta$ –O $\beta$	3.13	2.83	2.87	3.69	3.29	3.30
cation–O $\beta$		2.06	2.02		2.87	2.81
U–(O $\alpha$ –O $\alpha'$ )–U	137.9	135.2	134.1	151.4	145.3	144.4

<sup>a</sup> X-ray distances are averaged.

if  $\text{K}^+$  is coordinated to **P**. In fact, complexation does not affect the core of the cluster since only the uranyl moieties are tilted toward the cation in order to maximize the interaction. Also, we confirm theoretically that the dihedral angle U–(O $\alpha$ –O $\alpha'$ )–U is bent in all structures as found by Sigmon et al.<sup>3</sup> even when no cation is coordinated. However, the experimental data are better reproduced if the corresponding cation is complexed to **S** and **P** with a deviation of only 1.1° and 0.9° for **S** and **P**, respectively. By forcing all planar uranium-peroxo configuration in an idealized  $D_{4h}$  **S** structure, this lies 16 kcal·mol<sup>-1</sup> above the *pseudo-C<sub>4v</sub>*.

Regarding the electronic structure of the **S** and **P**, the main feature observed in the dimer, i.e., a typical polyoxometalate-like pattern, is found here too. The shape of the f orbitals enables the enhanced overlap between the  $\pi^*$  orbital of the O–O bridging unit and the uranium metal atoms observed in the dimer now is extended, which creates favorable metal–metal interactions through the bridges. Note in Figure 6 the shape of HOMO-3 in **S** and the HOMO-4 in **P** that suggest a sort of charge delocalization among all the uranium atoms.

Allowed symmetry combinations complete the occupied set of orbitals, which in all cases generates bonding interactions between two or three uranium atoms. This would explain the high stability of these building blocks. Indeed, the formation energy of a  $[\text{UO}_2(\text{O}_2)(\text{H}_2\text{O})_n]$  cycle by condensation of neutral monomers  $[\text{UO}_2(\text{O}_2)(\text{H}_2\text{O})_3]$  according to the reaction:



is computed as being exothermic in both cases by  $-16.9 \text{ kcal}\cdot\text{mol}^{-1}$  and  $-23.8 \text{ kcal}\cdot\text{mol}^{-1}$ , for **S** and **P**, respectively. The formation energy per uranyl unit,  $-4.2$  for **S** and  $-4.8$  for **P**, provides values more suitable for comparison and indicates a slight additional stabilization for **P**.

**Hexagonal  $[\text{UO}_2(\mu-\text{O}_2)(\text{H}_2\text{O})_6$  Building Blocks.** Similarly, we considered hexagonal building blocks. Unlike **S** and **P**, **H** adopts a variety of geometries ranging from planar conformations of the uranium atoms, like in  $\text{U}_{28}$  and  $\text{U}_{60}$ , to boat conformations like in  $\text{U}_{44}$ . The boat configuration closely resembles the cluster fragment isolated by Sigmon et al.<sup>3</sup> However, the X-ray data show a great variety of hexagonal conformations in between the planar and boat conformations. In addition to the boat (**H1**) and the planar (**H2**) conformations, we characterized a chairlike structure (**H3**), as it is shown in Figure 7. The three conformations are nearly degenerate in energy, the boat (**H1**) one being the most stable, which is followed by **H2** ( $+1.02 \text{ kcal}\cdot\text{mol}^{-1}$ ) and by **H3** ( $+1.45 \text{ kcal}\cdot\text{mol}^{-1}$ ). These values clearly suggest that the hexagonal macrocycle is geometrically flexible, as it is found in the X-ray structures. Formation of hexagonal macrocycles is exothermic too ( $-25 \text{ kcal}\cdot\text{mol}^{-1}$ ), and the formation energy per uranyl unit ( $-4.2 \text{ kcal}\cdot\text{mol}^{-1}\cdot\text{U-atom}^{-1}$ ) is very similar to the values found for **S** and **P**. Coordination of any cation can thus easily modify the geometry and thus alter the stability order. In other words, the

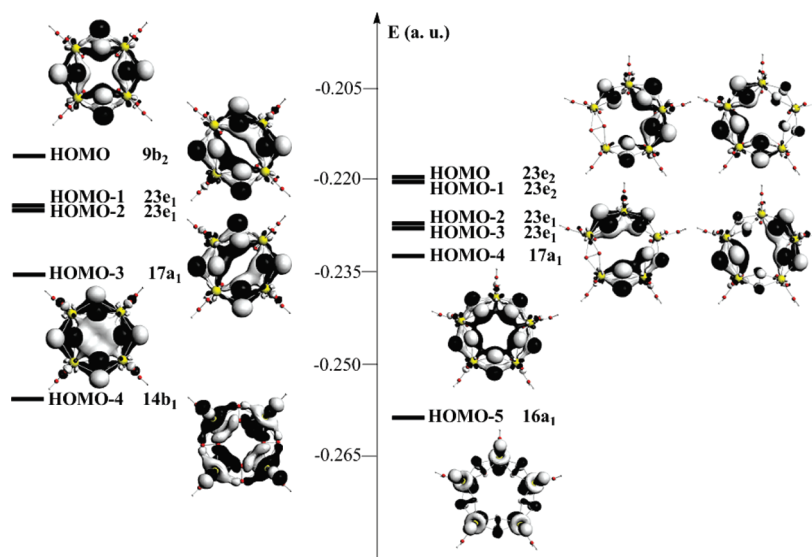


**Figure 6.** Highest occupied molecular orbitals for  $[(\text{UO}_2)_4(\text{O}_2)_4]$  (**S**) (left) and  $[(\text{UO}_2)_5(\text{O}_2)_5]$  (**P**) (right).

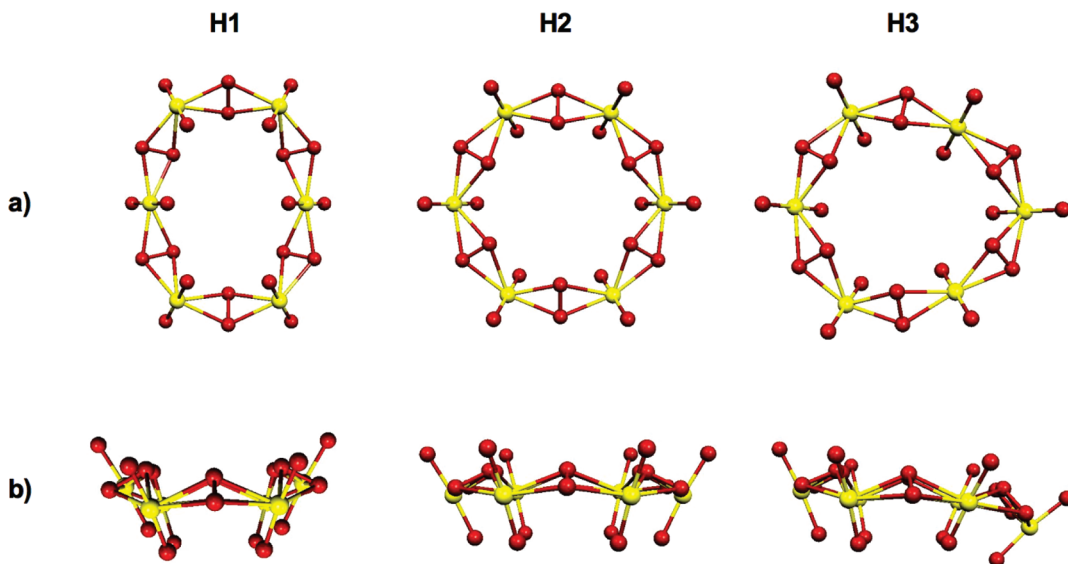


**Figure 7.** Molecular structures of the boat (**H1**), planar (**H2**), and chair (**H3**) conformations of  $[(\text{U}^{\text{VI}}\text{O}_2)_6(\text{O}_2)_6(\text{H}_2\text{O})_6]$ . (a) top view and (b) side view. Water molecules coordinated to U atoms are omitted for clarity. U yellow, O red.

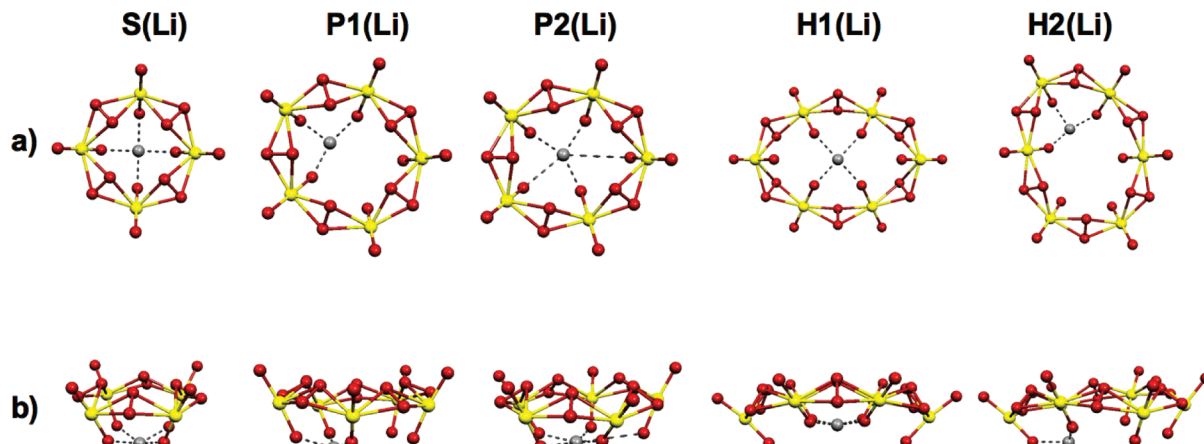


**Figure 8.** Molecular structures **S**, **P**, and **H** complexes with  $\text{Li}^+$ . (a) top view, (b) side view. Water molecules coordinated to U atoms are omitted for clarity. U yellow, O red, cation gray.

hexagonal macrocycle is flexible enough to adopt the conformation that suits best the requirements of a given counterion.

**Coordination of Alkali Cations.** The geometrical parameters for **S(Li)** and **P(K)** presented above demonstrate that the computational method used reproduces fairly well the structure of these isolated moieties compared to the X-ray structures found in nanoclusters. Then, we investigated the coordination of all alkali cations, from  $\text{Li}^+$  to  $\text{Cs}^+$ , to the **S**, **P**, and **H** macrocycles, we determined the most stable geometry, and computed and decomposed the complexation energy.

Geometries for the complexes **S(M<sup>+</sup>)** did not reveal any special feature: the cation sits in the center of the square, as shown in Figure 8 for **S(Li)**, and the  $\text{M}^+ - \text{O}\beta$  bond length elongates when the radii of  $\text{M}^+$  increases ( $\text{Li}$ : 2.065;  $\text{Na}$ : 2.416;  $\text{K}$ : 2.741;  $\text{Rb}$ : 2.943;  $\text{Cs}$ : 3.049 Å). This trend is not strictly followed by the  $\text{O}\beta - \text{O}\beta$  distances, which seem to reach an upper limit for the largest cations ( $\text{Li}$ : 2.830;  $\text{Na}$ : 3.043;  $\text{K}$ : 3.115;  $\text{Rb}$ : 3.124;  $\text{Cs}$ : 3.124 Å). Note that this limit value is very close to the value computed for the naked **S** (3.133 Å), which indicates that, although the uranyl-peroxo framework is flexible, it cannot accommodate those large cations without suffering tension. Consequently, the distance between the cation and the plane defined by the four  $\text{O}\beta$  oxygen increases as the size of the cation, from 0.534 Å for  $\text{Li}^+$  to 2.098 for  $\text{Cs}^+$ .

For **P(M<sup>+</sup>)**, except  $\text{Li}^+$ , the cation is optimally located in the center of the pentagon as shown in Figure 9 for **P(Na)**. For  $\text{Li}^+$ , we found two coordination modes: **P1(Li)** and **P2(Li)**, as depicted in Figure 8, **P1** being more stable than **P2** by 3.8 kcal·mol<sup>-1</sup>. In **P1(Li)**, the cation is coordinated to three adjacent uranyl  $\text{O}\beta$  oxygen atoms with bond lengths of 1.973, 2.030, and 2.039 Å, whereas in **P2(Li)** three distances are short (2.053, 2.100, 2.100 Å), one is medium (2.655 Å) and one long (3.448 Å). Coordination of the lithium cation strongly deforms the pentagonal shape, which is too large to hold the smallest cation comfortably in the center of the ring.

The highest flexibility of naked hexagons puts forth an even larger variety of coordination scenarios. Actually, two modes were found for  $\text{Li}^+$ : **H1(Li)**, where the cation is coordinated to four  $\text{O}\beta$  oxygens, and **H2(Li)** that resembles the tricoordinated species **P1(Li)**. As can be observed in Figure 8, bond lengths to  $\text{O}\beta$  oxygens are symmetrically distributed in both structures, even more than in the pentagon, with an average distance of 2.09 Å. **H1** is only 1.9 kcal·mol<sup>-1</sup> more stable than **H2**. For  $\text{Na}^+$  two coordination modes were found too, as well as for  $\text{K}^+$ ,  $\text{Rb}^+$ , and  $\text{Cs}^+$ , which are shown in Figure 9. **H1(Na)** is equivalent to **H1(Li)**, with four equivalent  $\text{Na} - \text{O}\beta$  contacts at 2.44 Å, and it is 4.9 kcal·mol<sup>-1</sup> more stable than **H2(Na)**, in which we found two  $\text{Na} - \text{O}\beta$  contacts at 2.45 Å.

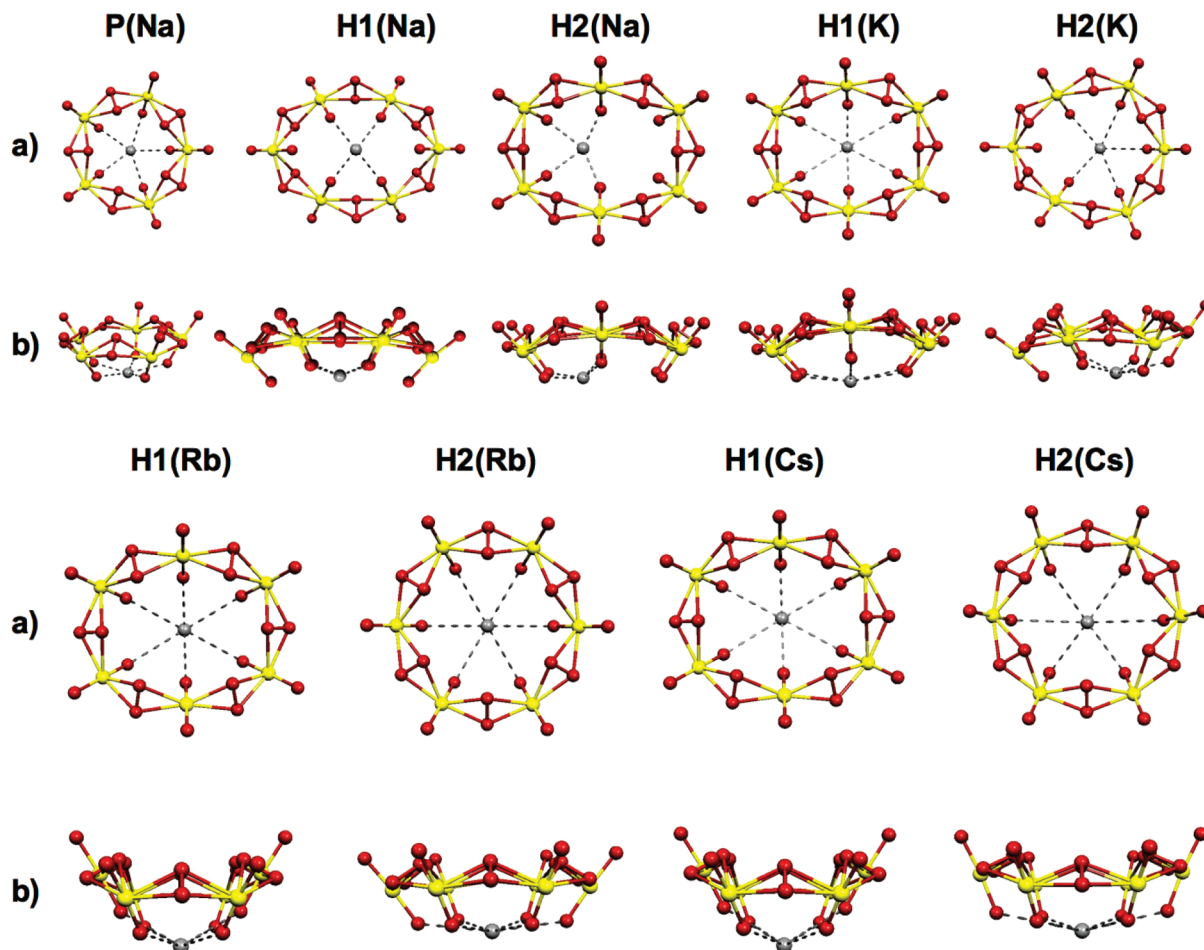


**Figure 9.** Molecular structures of several pentagonal and hexagonal complexes with Na, K, Rb, and Cs cations. (a) top view, (b) side view. Water molecules coordinated to U atoms are omitted for clarity. U yellow, O red, cation gray.

and two at 2.48 Å. For these two smaller cations, the flexibility of the hexagonal cycle is large enough to allow a boat-like conformation, but with an inverted curvature with respect to the naked hexagon. Note that the deformation of the hexagonal shape is clearly manifested in the angle formed by an uranyl unit and two next peroxy bridges: in the H1 conformation, we found four uranyls forming an angle  $U\text{--centroid}_{\text{peroxo}}\text{--}U$  of  $\sim 160^\circ$  and two of  $\sim 109^\circ$ , while in H2, it is the other way around, i.e., two wide and four narrow ones.

The potassium cation exhibits a higher tendency to coordination numbers five and six than sodium and lithium. The conformation adopted by the hexagonal macrocycle formed, which maximizes contacts with  $O\beta$  oxygens, is not as deformed as in the smaller cations. Therefore, we found the H1 boat-like conformer with two short contacts at 2.72 Å, and four at 3.27 Å, which is only slightly favored over the H2 chairlike conformation by 0.5 kcal·mol<sup>-1</sup>. In this chairlike structure,  $K^+$  directly interacts with five  $O\beta$  oxygens, forming an almost regular pentagon (average distance 2.95 Å), the sixth and longest one being at 3.90 Å.

Rubidium and cesium have never been used in experiments but seem to fit best into the hexagonal uranyl macrocycles. In both cases, in addition to the H1 boat-like structure, we characterized an almost flat, pseudo  $C_{6v}$  conformation H2, in which the hexagon is the least distorted. Averaged distances from cation– $O\beta$  oxygens are as follows: H1(Rb): 3.31, 2.91; H2(Rb): 3.23; H1(Cs): 3.20, 3.78; and H2(Cs): 3.02, 3.37 Å. While for Cs the hexagon H2 is slightly distorted, it shows perfect regularity for Rb. Energy differences between both conformers are small, 2.7 kcal·mol<sup>-1</sup> favoring H1(Rb) and 1.1 in favor of H2(Cs).

**Table 3.** Complexation Energies (in kcal·mol<sup>-1</sup>) of the S, P, H1, and H2 Macrocycles with Li<sup>+</sup>, Na<sup>+</sup>, K<sup>+</sup>, Rb<sup>+</sup>, and Cs<sup>+</sup>

cations	Li <sup>+</sup>	Na <sup>+</sup>	K <sup>+</sup>	Rb <sup>+</sup>	Cs <sup>+</sup>
S	-19.2	-22.1	-14.9	-11.5	-11.3
P	-10.4	-23.4	-18.8	-14.9	-15.6
H1	-6.0	-15.9	-15.4	-13.4	-13.7
H2	-8.9	-20.0	-15.9	-11.8	-15.8

Table 3 displays the complexation energy of the S, P, and H macrocycles with the alkali cations, defined as the formation energy of the complex with respect to separated components. The complexation energy corresponds to the stabilization induced by the pairing of the alkali cations to the naked S, P, and H macrocycles in their most stable conformation. First we discuss the S and P macrocycles under which cations were observed experimentally. The results indicate that S prefers to pair to Na<sup>+</sup> and Li<sup>+</sup> over Rb<sup>+</sup>, Cs<sup>+</sup>, or K<sup>+</sup>. Indeed Na<sup>+</sup> and Li<sup>+</sup> cations stabilize S by 22.1 and 19.2 kcal·mol<sup>-1</sup>, respectively. However, P favors the pairing to Na<sup>+</sup> and to K<sup>+</sup> over Cs<sup>+</sup>, Rb<sup>+</sup>, and Li<sup>+</sup>. Na<sup>+</sup> and K<sup>+</sup> stabilize P by 23.4 and 18.8 kcal·mol<sup>-1</sup>, respectively. Na<sup>+</sup> shows similar preference for S and for P, but stronger for P, while Li<sup>+</sup> clearly prefers S and K<sup>+</sup> prefers P. These results are fully consistent with the experimental data available (See Table 1) that show the existence of square face topologies with Li<sup>+</sup> and Na<sup>+</sup> and of pentagonal faces with Na<sup>+</sup> and K<sup>+</sup>. These conclusions seem also to be valid when a mixture of alkali cations is used in a competitive experiment. For example, in the case of U<sub>60</sub>, both Li<sup>+</sup> and K<sup>+</sup> are used during the synthesis but only P(K<sup>+</sup>) is identified. Here the difference between S(Li<sup>+</sup>) and P(K<sup>+</sup>) is rather small (0.3 kcal·mol<sup>-1</sup>), which

suggests that the higher inherent stability of the pentagonal building blocks might also play a role. **S(Na<sup>+</sup>)** is observed in U<sub>40</sub>, even though Li<sup>+</sup> is present in the medium.<sup>13</sup> In the case of U<sub>44</sub>, both **P(Na<sup>+</sup>)** and **P(K<sup>+</sup>)** are observed. However, the difference in the complexation energy between **P(Na<sup>+</sup>)** and **P(K<sup>+</sup>)** is not too large, and the distribution of the cations in the fully peroxide pentagonal faces of U<sub>44</sub> is not random. Indeed the same ratio of Na<sup>+</sup> and K<sup>+</sup> is present and **P(Na<sup>+</sup>)** is only observed under the faces at the tops of the capsule, while K<sup>+</sup> is located under the remaining pentagonal faces. This suggests that some other criteria might be responsible, in some cases, for the pairing of the cations to the different faces.

Regarding the influence of the alkali cations on the stability of the **H** building blocks, in general, both **H1** and **H2** are not as stabilized as **S** and **P** by complexation of the alkali cations. Na<sup>+</sup> seems to be able to bind **H2** with comparable strength. Only in the case of K<sup>+</sup>, the **H** structures are slightly more stabilized by the complexation of the cation than **S**. But **P(K<sup>+</sup>)** is still more stable than the **S** and **H** with K<sup>+</sup> by at least 4 kcal·mol<sup>-1</sup>. Moreover, there are very few **H** building blocks with only peroxide groups bridging the uranium atoms together, unlike in the case of **S** and **P**. In most cases, hexagonal faces present two or three hydroxide groups and the remaining peroxide bridges are shared with fully peroxide **S** or **P** faces.<sup>1–4</sup> This fact, coupled with the flexibility of the hexagonal macrocycle suggests that within the nanocapsule system **H** are merely linkers between more stable face topologies, in analogy with the Mo<sub>132</sub> polyoxometalate.<sup>11</sup>

Rb<sup>+</sup> and Cs<sup>+</sup> have never been used experimentally as far as we know. Note that Rb<sup>+</sup>, in contrast with the smaller cations, is almost indifferent to the face it can be complexed to, with a slight preference for **P** and **H** faces. Cs<sup>+</sup> behaves very similarly to Rb<sup>+</sup>, but with small preference for **H** rather than for **P**. This latter cation, together with Na<sup>+</sup>, appears in some open crown and bowl-shaped clusters<sup>5</sup> where, in addition to peroxide-hydroxide mixed hexagons, fully peroxide-bridged **S** are formed in U<sub>16</sub> as well. Thus, in this bowl-shaped system, Na<sup>+</sup> promotes the formation of the square faces whereas Cs<sup>+</sup> is complexed to the hexagonal faces.

The energy decomposition analysis scheme introduced by Rauk and Ziegler<sup>30</sup> has proven to be a very useful tool for discussing bonding in a number of systems.<sup>31–33</sup> The bonding energy  $\Delta E$  between two fragments is defined as the sum of three terms:  $\Delta E = \Delta E_{\text{Pauli}} + \Delta E_{\text{elst}} + \Delta E_{\text{oi}}$ , where the two first terms are computed by considering the unperturbed fragments and they account for the Pauli (steric) repulsion  $\Delta E_{\text{Pauli}}$  and electrostatic interaction  $\Delta E_{\text{elst}}$ , while the third term  $\Delta E_{\text{oi}}$  is the energy released when densities are allowed to relax. We analyzed the interaction between the alkali cations and **S** following the fragment approach,<sup>16</sup> and collected the various energy terms in Table 4.

As expected, Pauli repulsion increases as the size of the cation does, while the attractive electrostatic interaction decreases. Therefore, we see nothing surprising with these trends. Orbital interactions are strongly negative, particularly for Li<sup>+</sup>, indicating important charge reorganization/transfer when the complex is formed. Following the cations electronegativity scale, charge transfer from the cycle to the cation exhibits the same trend as  $\Delta E_{\text{oi}}$ . Indeed, final Mulliken atomic charge for the cation in the complex (0.76, 0.77, 0.88, 0.86, and 0.96 from Li<sup>+</sup> to Cs<sup>+</sup>) explains that the largest value obtained for  $\Delta E_{\text{oi}}$  corresponds to the most electronegative cation, for which charge transfer occurred to the greatest extend. Consequently, by adding the three terms, the largest  $\Delta E$  is computed for Li<sup>+</sup>, -108.4 kcal·mol<sup>-1</sup>, which is a huge value compared to the data presented in Table 3. The reader must be aware that energy decomposition analysis is computed in the gas phase, and that

**Table 4.** Interaction Energy Decomposition Analysis Terms (in kcal·mol<sup>-1</sup>) for **S** with Li<sup>+</sup>, Na<sup>+</sup>, K<sup>+</sup>, Rb<sup>+</sup>, and Cs<sup>+</sup>

	S(Li)	S(Na)	S(K)	S(Rb)	S(Cs)
electronic interactions					
$\Delta E_{\text{Pauli}}$	18.1	18.1	20.4	17.8	21.6
$\Delta E_{\text{elst}}$	-74.7	-65.6	-54.9	-48.1	-46.8
$\Delta E_{\text{oi}}$	-51.7	-30.3	-24.3	-20.3	-23.8
$\Delta E$	-108.4	-77.9	-58.8	-50.6	-49.0
solvation energies					
complex	-128.9	-129.2	-132.9	-135.0	-133.8
cation	-107.8	-71.1	-61.8	-58.7	-55.3
macrocycle	-111.0	-111.7	-111.1	-110.3	-110.9
$\Delta E_{\text{Solvation}}$	89.9	53.6	40.0	33.9	32.5
$\Delta E + \Delta E_{\text{Solvation}}$	-18.5	-24.3	-18.8	-16.7	-16.5

solvation effects are lacking. Therefore, solvation free energies computed for the complex, the alkali cation and the naked **S** are collected in Table 4 as well, where we can observe the energy penalty that has to be paid for desolvating the cations. In all of the cases, the sign of the solvation energies when the complex is formed,  $\Delta E_{\text{Solvation}}$ , is positive. Note that the trend is determined by the solvation energy of the cation since the solvation energy of the complex and of the naked macrocycle keep nearly constant along the series. Hence, when we take both energies into account (electronic + solvation), the bonding energy values obtained correspond to those collected in Table 3, but not exactly, because electronic energies were computed there including solvent effects self-consistently (for instance, 18.5 vs 19.3 for Li<sup>+</sup>). In any case, a subtle balance between the intrinsic interaction cation-macrocycles and the desolvation-solvation process needed to form the complex determines the complexation energies in Table 3. Although these values explain the preference of alkali metals for **S** and/or **P** building blocks, and the flexibility of **H**, and even allow making predictions in a qualitative way, they are not free from uncertainty. Computing solvation energies is the main source of error in the method used, therefore, a proper treatment of solvent effects is crucial.

## Conclusions

The results of our study confirm that the square **S**, pentagonal **P**, and hexagonal **H** building blocks are stable species under normal conditions. Molecular structures of neutral uranyl [UO<sub>2</sub>( $\mu$ - $\eta^2$ : $\eta^2$ -O<sub>2</sub>)(H<sub>2</sub>O)]<sub>n</sub> macrocycles are in good agreement with the X-ray geometric parameters found in polyanionic nanocapsules. Moreover, the accord is perfect when one cation is coordinated to our model systems. The inherent bent structure of the U–O<sub>2</sub>–U moiety is demonstrated in a cationic dimer, in which electronic effects were identified as the origin of the bending. In the **S**, **P**, and **H** building blocks we also observed that, even when no cation is present, the axes of the uranyl moieties are not perpendicular to the uranium atoms plane but tilted, with one set of the oxygen atoms (O $\beta$ ) slightly pointing toward the center of the polygon. This inherent curvature of the macrocycle minimizes repulsion between adjacent O $\alpha$  peroxy oxygens, and optimizes the overlap between uranium and peroxy units, enhancing charge delocalization in the cycle. The curvature is increased by cation coordination, thus we suggest that this is the driving force for constructing the building blocks with suitable geometry to self-assemble into nanocapsules *a posteriori*. However, **H** building blocks, which present different conformations ranging from chair to boat, are not as stabilized by the complexation of alkali cations.

Furthermore, we demonstrate the strong affinity of the **S** and **P** building blocks for Na<sup>+</sup>. If no sodium is present in the medium, then **S** prefers to bind to Li<sup>+</sup> while **P** favors coordination to K<sup>+</sup>. This is in full agreement with experimental

(30) Rauk, A.; Ziegler, T. *Inorg. Chem.* **1979**, *18*, 1558.

(31) Bickelhaupt, F. M.; Baerends, E. J. *Angew. Chem., Int. Ed.* **2003**, *42*, 4183–4188.

(32) Krapp, A.; Bickelhaupt, F. M.; Frenking, G. *Chem.—Eur. J.* **2006**, *12* (36), 9196–9216.

(33) Vyboishchikov, S. F.; Krapp, A.; Frenking, G. *J. Chem. Phys.* **2008**, *129* (14), 144111.

findings. The fact that in the latest new structures published by Burns' group, **S** and **P** building blocks are linked by other anions (pyrophosphate and methylenediphosphonate<sup>6</sup> and oxalate<sup>7</sup>), reinforces the idea of the higher stability of **S** and **P**. Triggered by interaction with the cations, this kind of building blocks form preferentially and are subsequently assembled into larger structures. In the U<sub>60</sub> structures, the hexagonal faces that form are mere linkers between the pentagonal building blocks. Following this idea, we suggest that experiments aimed at controlling the formation of stable building blocks templated by cations will then have the chance to grow larger clusters.

The complexation energy can be split into two terms: (i) intrinsic interaction, which is mainly electrostatic but with non-negligible charge transfer component for the smaller and more electronegative cations, and (ii) a desolvation/solvation term, mainly dominated by the cation solvation energy. As it was acknowledged a long time ago, this is a fundamental problem in chemistry<sup>34</sup> and biochemistry.<sup>35</sup> In this way, the interplay of these two factors makes it difficult to predict which nanocapsule will be formed from a mixture of cations. Although the interaction with Li<sup>+</sup> is the strongest, this cation is unwilling to lose its solvation shell. This could explain, for instance, the new structures reported by Nyman<sup>36</sup> where water-bridge lithium cluster encapsulating [UO<sub>2</sub>(O<sub>2</sub>)<sub>3</sub>]<sup>4-</sup> was characterized (ULi<sub>16</sub>). However, for those nanocapsules having K<sup>+</sup> as counterion, we would suggest that a Na<sup>+</sup>/K<sup>+</sup> exchange phenomena could occur

without disturbing the structure because pentagonal and hexagonal pores are large enough to allow cations to pass through.

Finally, for Rb<sup>+</sup> we predict a similar behavior as for Cs<sup>+</sup>: the largest cation should preferably bind to hexagons. In the U<sub>28</sub> structure reported by Burns,<sup>1</sup> potassium cations appear under pentagonal and hexagonal faces. According to the results collected in Table 3, it is expected that if a mixture of K<sup>+</sup> and Cs<sup>+</sup> is used during the synthetic procedure, K<sup>+</sup> would likely interact with pentagonal faces while Cs<sup>+</sup> would with hexagonal faces.

We have a long way to go until the growth mechanism of these uranyl peroxide nanoclusters is fully understood. Although the chemistry of polyoxometalates caused myriads of nanostructures to bloom, the formation mechanism of one of the smallest polyoxometalate [W<sub>6</sub>O<sub>19</sub>]<sup>2-</sup> has been proposed only very recently.<sup>37</sup> Further studies will be carried out in this direction.

**Acknowledgment.** Research supported by the MICINN of Spain (CTQ2008-06549-C02-02/BQU and Consolider Ingenio 2010 CSD2006-0003), the CIRIT of the Catalan Government (2009SGR259) and the ICIQ Foundation. Computer resources provided by the BSC-CNS. P.M. thanks the Generalitat de Catalunya for an FI fellowship (2009FIC00026).

**Supporting Information Available:** Cation solvation radii and energies, Cartesian coordinates and binding energy of the structures, molecular orbitals for the dimer. This material is available free of charge via the Internet at <http://pubs.acs.org>.

JA1053175

- (34) Glendening, E. D.; Feller, D.; Thompson, M. A. *J. Am. Chem. Soc.* **1994**, *116* (23), 10657–10669.  
(35) Hud, N. V.; Smith, F. W.; Anet, F. A. L.; Feigon, J. *Biochemistry* **1996**, *35* (48), 15383–15390.  
(36) Nyman, M.; Rodríguez, M. A.; Campana, C. F. *Inorg. Chem.* **2010**, *49* (17), 7748–7755.

- (37) Vilà-Nadal, L.; Rodríguez-Fortea, A.; Yan, L. K.; Wilson, E. F.; Cronin, L.; Poblet, J. M. *Angew. Chem., Int. Ed.* **2009**, *48*, 5452.